# Imaging and characterizing damages in metallic plates using Lamb waves

\*C.T. Ng

School of Civil, Environmental & Mining Engineering, The University of Adelaide, SA, Australia.

\*Presenting author: alex.ng@adelaide.edu.au

## **Abstract**

The paper presents a study for quantitative imaging of damage in metallic plates using the fundamental anti-symmetric mode of  $(A_0)$  Lamb wave. The study proposed a two-stage approach, in which the damage location is first determined in stage-one through analyzing the cross-correlation of the excitation pulse and scattered wave signal, and the damage is then characterized in stage-two using the Mindlin plate theory based Lamb wave diffraction tomography. The damage considered in this study is an elliptical shape of plate thickness reduction, which is a simplified representation of corrosion damage in metallic plates. The two-stage approach is employed to quantitatively image the plate thickness reduction, i.e. determine the location, size and shape of the thickness reduction. Finite element simulation of a circular transducer network with eight transducers is used to demonstrate the capability of the two-stage approach in characterizing the damage. The results show that the two-stage approach is able to accurately identify the damage location and provide a reasonable estimation of the size and shape of the damage.

**Keywords:** Lamb wave, diffraction tomography, scattering, imaging, damage characterization, structural health monitoring

#### Introduction

Structural health monitoring (SHM) is a process of monitoring the performance and evaluating the state of health of structures based on measurements. It can be used to ensure the safety and sustainability of structures and have been widely employed in different engineering fields, such as civil, mechanical and aerospace engineering. Lamb wave based approach has been widely recognized as one of the promising techniques for damage detection, and hence, to ensure the structural safety (Alleyne et al 2001; Veidt and Ng 2011; Ng and Veidt 2012). The advantages of using Lamb wave in damage detection are its high sensitive to most types of damage, efficient in detecting small and subsurface damage, and capable for inspecting large structure areas. In the last decade, different Lamb wave based methods have been developed for damage inspection. Apart from the essential requirement that damage inspection systems must be reliable, two highly desirable features are the graphic representation and quantitative damage identification.

Lamb wave based tomographic approach is one of the techniques that can achieve the aforementioned desirable features. Early developments focused on the use of the time-of-flight information to reconstruct an image for damage identification (Jansen and Hutchins 1990; Malyarenko and Hinder 2001; Leonard and Hinders 2005; Belanger et al. 2010; Huthwaite and Simonetti 2013). A Mindlin plate theory based Lamb wave diffraction tomography framework was proposed by Wang and Rose (2003). The framework reconstructs the damage image through Born approximation of the Lamb wave scattering from the damage and the inversion is solved by direct Fourier inversion approach. Rohde et al. (2009) then demonstrated the damage imaging reconstruction could be achieved using eight transducers through the far-field Born approximation. Recently Rose and Wang (2010) proposed a filtered back-propagation algorithm to solve the inverse problem in the Lamb wave diffraction tomography. They demonstrated that the filtered back-propagation algorithm in reconstructing the damage image is more robust and computationally efficient.

This study employs a two-stage approach to reconstruct the elliptical shape of plate thickness reduction in metallic plates, which demonstrates the capability of the approach in imaging the damage size and shape. The paper is organized as follows. The proposed two-stage approach is first described in the first section. The numerical verification using a three-dimensional (3D) explicit finite element (FE) simulation is then described and the results are discussed in detail. Finally, conclusions are drawn in the last section.

## Two-stage imaging approach

The two-stage imaging approach relies on collecting Lamb wave data through a distributed transducer network with N transducers. Each of these transducers can act as actuator and sensor for actuating and sensing the Lamb waves. In the damage detection process, the network of transducers is used to sequentially scan the structure before and after the presence of the damage by transmitting and receiving Lamb waves. In each scan, one of the transducers is used to excite the  $A_0$  Lamb wave and the rest of the transducers are used to measure the Lamb wave signals. In each sequential scan process, there are in total of N(N-1) actuator-sensor signal paths. Once the data of before and after the presence of the damage is collected, a baseline subtraction process is then used to extract the scattered wave signals (Ng and Veidt 2011)

$$u^S = u^D - u^{UD} \tag{1}$$

where  $u^{UD}$  and  $u^D$  are the signals measured before and after the presence of the damage.  $u^S$  is the scattered signal extracted using the baseline subtraction process. The scattered signals are then used in the two-stage approach to reconstruct the damage.

In the stage-one, the targeted inspection area is discretized into a set of image pixels located at (x,y). Considering two of the transducers in the transducer network as an example, the intensity of the image pixel  $(I_{ab})$  at (x,y) contributed by the actuator/sensor signal path a-b (two of the transducers in the network) can be calculated as (Wang et al. 2005; Ng and Veidt 2009)

$$I_{ab}(x,y) = C_{ab} \left( \frac{\sqrt{(y_b - y)^2 + (x_b - x)^2} + \sqrt{(y - y_a)^2 + (x - x_a)^2}}{c_g} \right)$$
(2)

where  $(x_a, y_a)$  and  $(x_b, y_b)$  is the location of transducer a and b, respectively. (x, y) is the location of image pixel.  $c_a$  is the group velocity of the fundamental asymmetric mode of Lamb wave.  $C_{ab}$  is the cross-correlation between the incident pulse generated by transducer a and the scattered wave signal measured by transducer b. In this study the wavelet coefficient calculated using the continuous Gabor wavelet transform (Kishimoto et al. 1995; Ng et al. 2009) is used in the cross-correlation to provide a reliable extraction of the scattered wave signal components at the excitation frequency. Once the image of each actuator-sensor signal path is reconstructed using Eq. (2), the image indicating the estimated damage location can then be reconstructed by superimposing the power flux of all images as

$$I(x,y) = \sum_{a=1}^{N} \sum_{b=1, b \neq a}^{N} A_{ab} I_{ab}^{2}$$
(3)

where  $A_{ab}$  is a weighting factor used to account for varying sensitivities of individual transducer and is equal to unity for uniform aperture weighting.

After the damage location is estimated in stage-one, the Mindlin plate theory based Lamb wave diffraction tomography is then employed to reconstruct the size and shape of the plate thickness reduction in stage-two. It is assumed that the damage is a weak inhomogeneity with a finite region  $\Sigma$ . The scattered flexural wave can be represented as follow using the Born approximation (Wang and Chang 2005)

$$\mathbf{u}_{B}^{S}(\mathbf{x},\boldsymbol{\omega}) = \iint_{S} \left[ s_{1}D\Gamma_{\beta\alpha}^{I} g_{3\alpha,\beta} + s_{2}\kappa^{2}Gh(\mathbf{u}_{\alpha}^{I} - \Omega_{\alpha}^{I}) (g_{3\alpha} + g_{33,\alpha}) + s_{3}\rho I\omega^{2}\Omega_{\alpha}^{I} g_{3\alpha} + s_{4}\rho h\omega^{2} g_{33} \right] d^{2}\xi$$
(4)

where  $\omega$  is the excitation frequency of the incident wave.  $D=Eh^3/12(1-\nu)^2$  is the flexural stiffness of the plate, where E, h and  $\nu$  are the Young's modulus, thickness and Poisson's ratio, respectively.  $\rho$  and G are the effective shear modulus and the density of the plate material.  $I=h^3/12$  is the through-thickness area moment.  $\kappa=\pi/\sqrt{12}$  is the shear correction factor for accurate representation of the low frequency behavior.  $s_n$ , for n=1,...,4, are parameter perturbations and have non-zero value for  $\mathbf{x} \in \Sigma$  but vanish for  $\mathbf{x} \notin \Sigma$ .  $\mathbf{x}$  is a position vector and  $\xi$  is an arbitrary point within the region  $\Sigma$ .  $u_n^{\ell}$  and  $\Omega_n^{\ell}$  are the plate-normal displacement and rotary deflections.  $\Gamma_n^{\ell}$  is the plate-theory strain. The comma indicates the differentiation between subscripts  $[\alpha, \beta] = 1, 2$ .  $g_{ij} = g_{ij}(\xi \mid \mathbf{x})$  is the dynamic Green's functions solution for wave scattering (Rose and Wang 2004; Ng et al. 2012). The scattered waves can be simplified using the far-field asymptotic expression of the Hankel function as

$$u_{B}^{S}\left(r_{s}, \theta^{S}, \theta^{I}, \omega\right) = \sum_{n=1}^{4} \left[P_{n}\left(k_{1}, \theta^{S} - \theta^{I}\right) \hat{S}_{n}\left(\mathbf{k}_{1}^{S} - \mathbf{k}_{1}^{I}\right) \sqrt{\frac{2}{\pi k_{1} r_{s}}} e^{i\left(k_{1} r_{s} - \frac{\pi}{4}\right)}\right]$$
(5)

where  $r_s = \sqrt{(x-\xi)^2 + (y-\eta)^2}$ .  $\theta^I$  and  $\theta^S$  are the angle of the incident and scattered waves, respectively.  $\mathbf{k}_1^I = k_1[\cos\theta^I, \sin\theta^I]$  and  $\mathbf{k}_1^S = k_1[\cos\theta^S, \sin\theta^S]$  denote the incident and scattered wave vector.  $k_1$  is the wavenumber evaluated using Mindlin plate theory.  $P_n$  for n = 1, 2, 3, 4 are defined as

$$P_{1}(k_{1},\theta) = -\frac{i\gamma k_{1}^{2}}{4(k_{1}^{2} + k_{2}^{2})} (\cos^{2}\theta + \nu \sin^{2}\theta)$$
 (6)

$$P_{2}(k_{1},\theta) = -\frac{i\kappa^{2}Ghk_{1}^{2}(1-\gamma)^{2}}{4D\gamma(k_{1}^{2}+k_{2}^{2})}\cos\theta$$
 (7)

$$P_3(k_1,\theta) = \frac{i\rho I\omega^2 \gamma k_1^2}{4D(k_1^2 + k_2^2)} \cos\theta \tag{8}$$

$$P_4(k_1,\theta) = \frac{i\rho h\omega^2}{4D\gamma(k_1^2 + k_2^2)} \tag{9}$$

where  $k_2$  is the wavenumber of the second possible wave mode in Mindlin plate theory.  $\gamma = i/4D(k_1^2 - k_2^2)$ .  $\hat{S}_n(\mathbf{k})$  is the two-dimensional Fourier transform of the perturbation functions and is defined as

$$\hat{S}_{n}(\mathbf{k}) = \iint_{\Sigma} s_{n}(\xi) e^{-i\mathbf{k}\cdot\xi} d\xi \tag{10}$$

In this study the focus is on the reduction of the plate thickness due to corrosion in metallic plate, and hence,  $3s_1(\xi) = s_2(\xi) = 3s_3(\xi) = s_4(\xi)$  is used in the image reconstruction. Once the  $\hat{S}_n(\mathbf{k})$  is calculated, the perturbation function  $s_n(\xi)$  can be obtained by carrying out the two-dimensional inverse Fourier transform as

$$s_n(\mathbf{x}) = \frac{1}{(2\pi)^2} \iint_{|\mathbf{k}| \le 2k_1} \hat{S}_n(\mathbf{k}) e^{-i\mathbf{k}\cdot\mathbf{x}} dk_x dk_y \tag{11}$$

where  $\mathbf{k} = [k_x, k_y] = [k_1(\cos\theta^S - \cos\theta^I), k_1(\sin\theta^S - \sin\theta^I)]$ . The obtained perturbation function can then provide a quantitative imaging of the damage.

#### **Numerical case studies**

A  $300\times300\times6\mathrm{mm}^3$  steel plate was modeled using 3D explicit FE simulation. The commercial FE software LS-DYNA was used in this study to carry out the FE simulation. The material properties of the steel are  $E=203\mathrm{GPa}$ , v=0.29 and  $\rho=7800~\mathrm{kg/m}^3$ . The steel plate was modeled using eightnoded 3D reduced integration solid brick elements with hourglass control. It is assumed that a 50mm radius circular transducer network was installed on the steel plate as shown in Fig. 1. The transducer network has eight piezoceramic transducers ( $T_1-T_3$ ) with 5mm diameter. The excitations generated by the transducers were modeled through applying the out-of-plane displacement to the surface nodal point covered by the piezoceramic transducers. The excitation signal is a 200kHz narrow band six-cycle sinusoidal tone burst pulse modulated by a Hanning window. In this study the  $A_0$  Lamb wave was excited and the wavelength was 11.99mm. The solid brick elements had inplane square shape with dimension  $0.75\times0.75\mathrm{mm}^2$  and the thickness was  $0.375\mathrm{mm}$ , and hence, the plate was modeled using 16 layers of solid element in the thickness direction.

Three damage cases, Cases E1 – E3, were considered in this study. Case E1 considered an elliptical thickness reduction with major axis length  $e_1 = 4$ mm and minor axis length  $e_2 = 2$ mm, respectively. In this case the major axis is along the x-axis as shown in Fig. 1. The thickness reduction was generated by removing a top and bottom layer of the solid element in the elliptical thickness reduction area. The total percentage of thickness reduction is 12.5%. As the thickness reduction was symmetrical about the mid-plane of the plate, there was no mode conversion effect in

the scattered waves. Cases E2 and E3 consider the same elliptical thickness reduction but the major axis direction was rotated 45° and 90° in anti-clockwise direction, respectively. All cases considered the center of the elliptical thickness reduction located at the center of the circular transducer network.

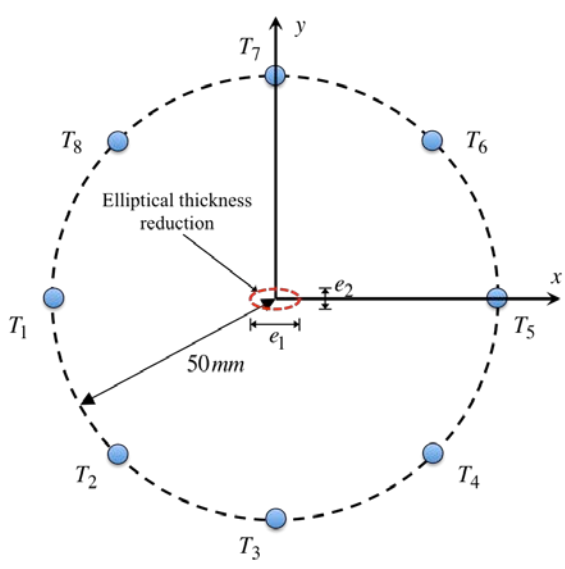


Figure 1. Transducer network and elliptical thickness reduction in the numerical case studies

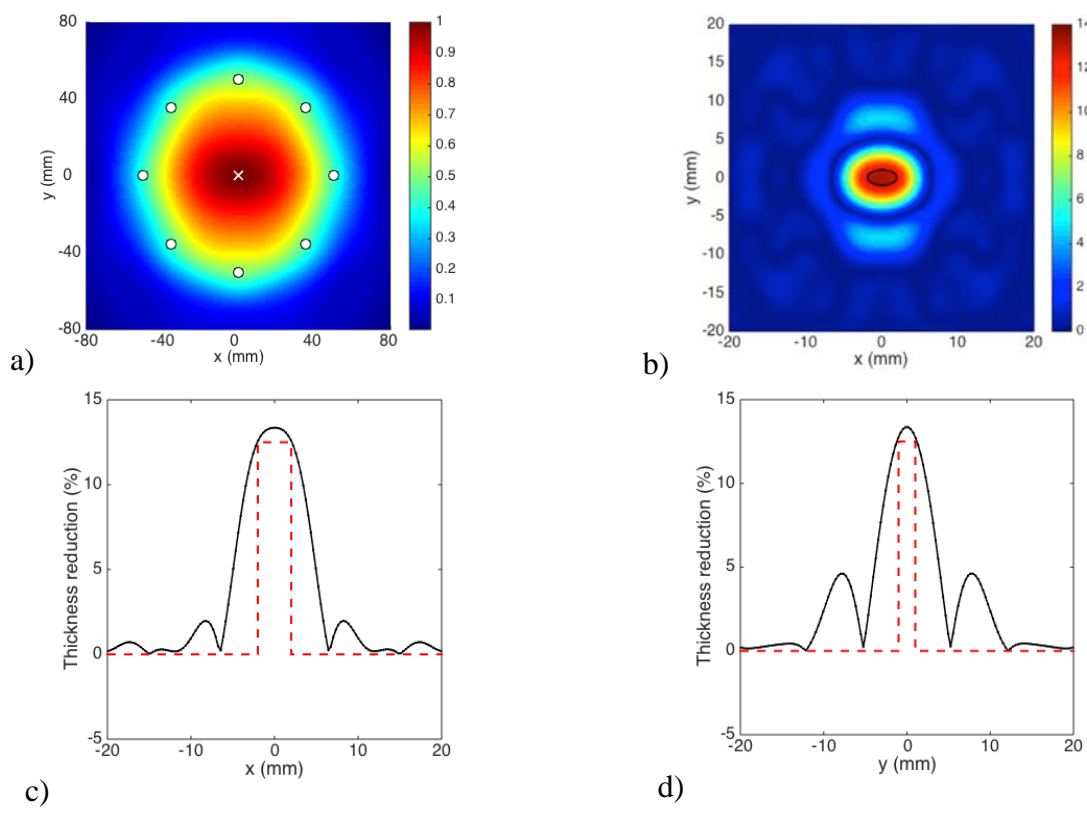


Figure 2. a) Reconstructed damage location image (white cross: actual damage location), b) reconstructed plate thickness reduction percentage image (close up view at the damage region (black ellipse: actual size and shape of the damage), and profile across the damage in c) x-axis and d) y-axis (black solid line: reconstructed thickness reduction percentage; red dashed line: actual thickness reduction percentage) for Case E1

Using the stage-one of the proposed methodology, a reconstructed damage location image for Cases E1, E2 and E3 are shown in Figs. 2a, 3a and 4a, respectively. The while circles indicate the transducer locations and the white cross indicate the center of the actual thickness reduction. The reconstructed damage location image correctly determines the actual damage location for all three

cases. Figs. 2b, 3b and 4b show the reconstructed plate thickness reduction percentage image using stage-two of the proposed methodology, i.e. the Lamb wave diffraction tomography. In these figures, the actual thickness reduction size and shape are indicated by black ellipses. The images show that there is a good agreement between the reconstructed and actual plate thickness reduction size and shape.

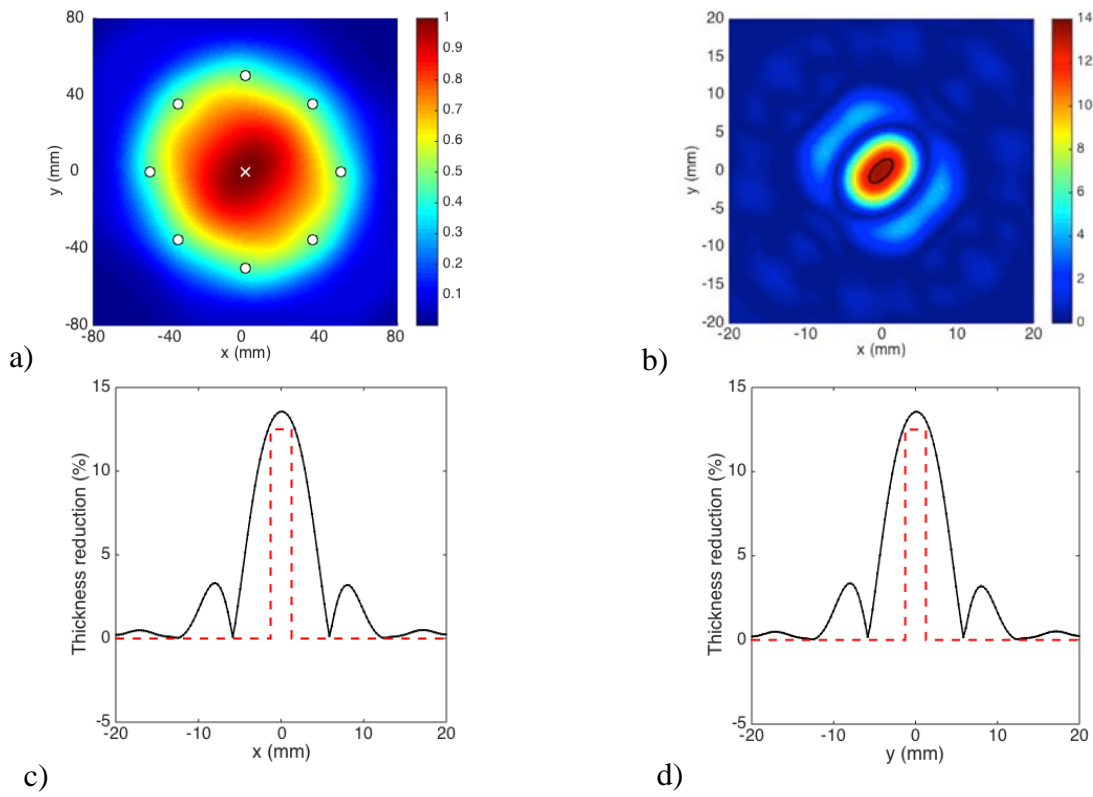


Figure 3. a) Reconstructed damage location image (white cross: actual damage location), b) reconstructed plate thickness reduction percentage image (close up view at the damage region (black ellipse: actual size and shape of the damage), and profile across the damage in c) x-axis and d) y-axis (black solid line: reconstructed thickness reduction percentage; red dashed line: actual thickness reduction percentage) for Case E2

Figs. 2c, 2d, 3c, 3d, 4c and 4d show the thickness reduction percentage profile across the damage for Cases E1 to E3. The black solid line is the reconstructed thickness reduction percentage and the red dashed line is the actual thickness reduction percentage. These figures show that the reconstructed profiles are able to provide a reasonable estimation of the actual thickness reduction percentage.

## **Conclusions**

This paper has presented study of employing a two-stage approach for quantitative imaging of damage in metallic plates. The damage type considered in this study is an elliptical thickness reduction. In stage-one of the approach, the location of the thickness reduction was first determined. The size and shape of the thickness reduction were then determined in stage-two using the Lamb wave diffraction tomography. Numerical cases studies have been carried out using the 3D explicit FE simulation. Three cases were considered in the study, which considered the same size of the elliptical thickness reduction but with different orientations of the major axis. The results show that the two-stage approach could accurately determine the damage location and provide a reasonable estimation of the size and shape of the thickness reduction.

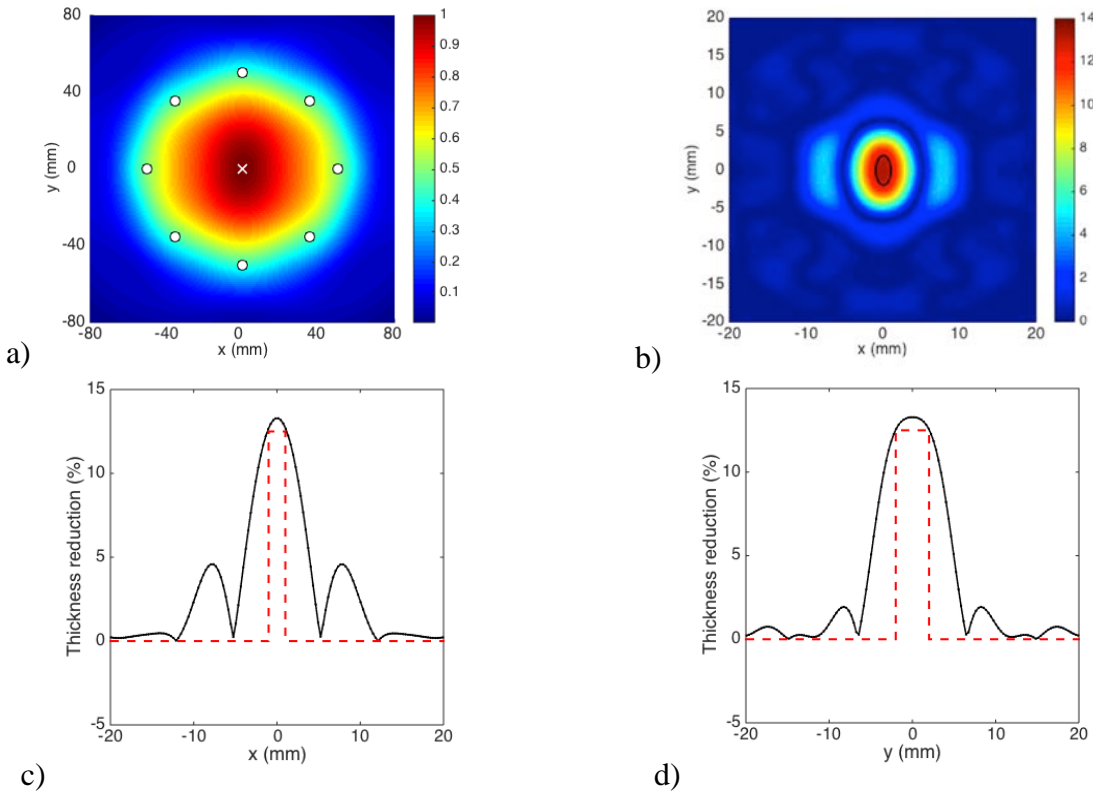


Figure 4. a) Reconstructed damage location image (white cross: actual damage location), b) reconstructed plate thickness reduction percentage image (close up view at the damage region (black ellipse: actual size and shape of the damage), and profile across the damage in c) x-axis and d) y-axis (black solid line: reconstructed thickness reduction percentage; red dashed line: actual thickness reduction percentage) for Case E3

## Acknowledgements

The research described in this paper was financially supported by the Australian Research Council under grant number DE130100261. The support is greatly appreciated.

## References

Alleyne D., Pavlakovic B., Lowe M. and Cawley P., Rapid, long range inspection of chemical plant pipework using guided waves, *Insight*, **43**(2): 93-96, 2001

Belanger P., Cawley P. and Simonetti F., Guided wave diffraction tomography within the Born approximation, *IEEE Transactions of Ultrasonics, Ferroelectrics and Frequency Control*, **57**(6): 1405-1418, 2010

Huthwaite P. and Simonetti F., High-resolution guided wave tomography, Wave Motion, 50: 979-993, 2013

Jansen, D.P. and Hutchins, D.A. (1990), "Lamb wave tomography", *IEEE Ultrasonics Symposium Proceedings*, Honolulu, HI, December 1017-1020.

Kishimoto K., Inoue H., Hamada M. and Shibuya T., Time frequency analysis of dispersive waves by means of wavelet transform, *Journal of Applied Mechanics*. **62**: 841-848, 1995

Leonard K.R. and Hinder M.K., Lamb wave tomography of pipe-like structures, *Ultrasonics*, **43**: 574-583, 2005

Malyarenko E.V. and Hinder M.K., Ultrasonic man wave diffraction tomography, *Ultrasonics*, 39(4): 269-281, 2001

Ng C.T. and Veidt M., A Lamb-wave-based technique for damage detection in composite laminates, *Smart Materials and Structures*, **18**(7)074006: 1-12, 2009

Ng C.T. and Veidt M., Scattering characteristics of Lamb waves from debondings at structural features in composite laminates, *The Journal of the Acoustical Society of America*, **132**(1): 115-123, 2012

Ng C.T. and Veidt M., Scattering of the fundamental anti-symmetric Lamb wave at delaminations in composite laminates, *The Journal of the Acoustical Society of Am*erica, **129**(3): 1288-1296, 2011

Ng C.T., Veidt M. and Rajic N., Integrated piezoceramic transducers for imaging damage in composite laminates, *Proceedings of SPIE*, **7493M**: 1-8, 2009

- Ng C.T., Veidt M., Rose L.R.F. and Wang C.H., Analytical and finite element prediction of Lamb wave scattering at delaminations in quasi-isotropic composite laminates, *Journal of Sound and Vibration*, **331**(22): 4870-4883, 2012
- Rohde A.H., Rose L.R.F., Veidt M. and Wang C.H., Two inversion strategies for plate wave diffraction tomography, *Materials Forum*, **33**: 489-495, 2009
- Rose J.L., A baseline and vision of ultrasonic guided wave inspection potential, *Journal of Pressure Vessel Technology*, **124**: 273-282, 2002
- Rose L.R. and Wang C.H., Mindlin plate theory for damage detection: imaging of flexural inhomogeneities, *The Journal of the Acoustical Society of America*, **127**(2): 754-763, 2010
- Rose L.R. and Wang C.H., Mindlin plate theory for damage detection: source solutions, *The Journal of the Acoustical Society of America*, **116**: 154-171, 2004
- Veidt M. and Ng C.T., Influence of stacking sequence on scattering characteristics of the fundamental anti-symmetric Lamb wave at through holes in composite laminates, *The Journal of the Acoustical Society of America*, **129**(3): 1280-1287, 2011
- Wang C.H. and Chang F.K., Scattering of plate waves by a cylindrical inhomogeneity, *Journal of Sound and Vibration*, **282**: 429-451, 2005
- Wang C.H. and Rose L.R.F., Plate-wave diffraction tomography for structural health monitoring, *Review of Progress in Quantitative Nondestructive Evaluation*, **22**: 1615-1622, 2003
- Wang C.H., Rose J.T. and Chang F.K., A synthetic time reversal imaging method for structural health monitoring, *Smart Materials and Structures*, **13**: 415-423, 2004